Journal of
Ceramic Science
and Technology

J. Ceram. Sci. Technol. 29-38 (2019)
DOI: 10.4416/JCST2018-00072
available online at: http://www.ceramic-science.com

Sol-Gel Synthesis of Strontium Titanate Nanofibers by Electrospinning

J. H. Roque-Ruiz[1], J. Meraz-Angel[1], R. Farias[2], M. Meléndez-Lira[3], S. Y. Reyes-López[*1].

[1]Instituto de Ciencias Biomédicas, Universidad Autónoma de Ciudad Juárez, Envolvente del PRONAF y Estocolmo s/n, Ciudad Juárez, Chih., México C.P. 32300
[2]Instituto de Ingeniería y Tecnología, Universidad Autónoma de Ciudad Juárez, Av. del Charro No. 450 Nte. Col. Partido Romero C.P. 32310
[3]Physics Department, CINVESTAV-IPN, Apdo. Postal 14 – 740 México, D.F. 07360, México
received June 28, 2018; received in revised form February 28, 2019; accepted March 15, 2019

Abstract

The preparation of homogeneous $SrTiO_3$ nanofibers has been difficult and there are few publications in this field. In this research, consistent structures of strontium titanate ceramic fibers were obtained using an easy sol-gel and electrospinning methodology, giving an alternative for preparing ceramics in the form of fibrillar membranes. Two sol-gel solutions starting from Strontium nitrate and titanium tetraisopropoxyde were prepared and then mixed and homogenized with polyvinylpyrrolidone polymeric solution. The green fibers obtained from the ceramic precursors had a diameter of 140 to 180 nm. At 1000 °C the shape of fibers was preserved, with mean diameter of 103±39 nm. Based on the thermal analysis, the phase transition from tetragonal titanium oxide to the perovskite structure of strontium titanate was determined to take place at 800 °C. By infrared spectroscopy, Raman spectroscopy and X-ray diffraction analysis, it was determined that ceramic fibers at 1200 °C had a perovskite structure characteristic of strontium titanate.

Keywords: electrospinning, perovskite, sol-gel, strontium titanate.

I. Introduction

Strontium titanate is a ceramic material, of the perovskite family, with semiconductor properties attributed to titanium oxide and amplified by addition of strontium [1]. Consequently, strontium titanate is used in the fabrication of electronic components. Since 1955 this ceramic is employed as gemstone [2]. However, the use of strontium titanate for manufacturing electronic components such as optical sensors, RAM, and transistors just gained attention at early 2000. Demand of strontium titanate has increased considerably. However, common processes used for obtaining this ceramic, for instance, Vermeuil method and mechanical milling, are slow and expensive. The first method (Vermeuil) requires high temperatures to obtain crystals, while by using the second (mechanical milling) ceramic powders are obtained [1–2]. Therefore, additional processes, such as pressing and sintering, are applied to these powders. Furthermore, the fabrication of diverse or complex structures requires further processing (extraction, preparation of slurries, drying and firing), increasing production costs.

As a result, the development of new synthesis and processing routes have gained interest. An important technique for the fabrication of advanced ceramic materials is the sol-gel process. This method improves the consolidation of green bodies at room temperature, reducing costs and processing times. Recently, there has been an intense research effort on electrospinning of ceramics, however, we were not able to find many reports on the synthesis of homogenous strontium titanate nanofibers by electrospinning [2–8]. Perovskite fibers with a general formula of ABO_3, such as $SrTiO_3$ have wide applications in various fields. Among them, $SrTiO_3$ is of great interest in the fields of substrates for thin film growth, water splitting catalysis, electronic devices and photocatalytic degradation of organic pollutants [1–2, 9–11].

Electrospinning is a simple and useful method for the fabrication of complex structures consisting of continuous fibers. Moreover, electrospinning is a simple and versatile technique, which can be used to obtain fibers with diameters down to tens of nanometers. Long, thin, solid fibers can be generated as the electrified jet is continuously stretched by electrostatic forces [2–8,12–15]. The morphology of electrospun fibers can be controlled by adjusting experimental parameters, such as the precursor solution concentration (viscosity), the type of spinneret, voltage and spinneret-collector distance. In this work, the preparation of precursor fibers by electrospinning of metal-organic solutions is reported. Processing parameters such as voltage, feeding rate, and needle-collector distance were optimized to obtain continuous fibers without defects. Furthermore,

* Corresponding author: simon.reyes@uacj.mx

as-spun samples were treated thermally to obtain dense strontium titanate fibers.

II. Materials and Methods

Sol-gel was prepared by dissolving 0.2 g of Strontium nitrate $Sr(NO_3)_2$ (Alfa Aesar 99%) and 3 mL of Acetic acid (Alfa Aesar) in deionized water. This solution was stirred magnetically for 1 h. Next, 0.6 mL of Titanium tetraisopropoxyde $C_{12}H_{28}O_4Ti$ (Sigma Aldrich 97%) were added dropwise and the solution (final Sr:Ti molar ratio was 1:1) was stirred for 1 h. Simultaneously, 3 mL of a 10% Polyvinyl pyrrolidone PVP (Alfa Aesar Mw 1,300,000) solution were prepared using ethanol (Jalmek 99.5%) as solvent. This solution was added to sol-gel and homogenized for 1 h. Two precursor solutions of 0.3 M concentration were used in electrospinning. The M1 sample was used as prepared, while the M2 was used after aging for 24 h. The precursor solutions were transferred to a 10 mL glass syringe (Fortuna ® Optima ®) with a steel needle and placed in a KD Scientific 230 injection pump. Needle-collector distance of 10 cm was used during electrospinning process. Feeding rate was 12 μL/min, while voltage was 9 kV. Fibers were collected on a rotating drum covered with aluminum foil. Environmental parameters during electrospinning process were 21 °C and 30% for Temperature and Relative Humidity, respectively. Characterization of as-spun fibers was carried out by Fourier Transformed Infrared Spectroscopy with a Bruker Alpha Platinum ATR instrument by Attenuated Total Reflection technique, with 40 scans and resolution of 4 cm^{-1} Morphology, diameters and Energy dispersive X-ray spectroscopy (EDX) were determined by Scanning Electron Microscopy with an instrument JEOL JSM-6010 PLUS/LA. Thermogravimetric analysis (TGA), Differential Thermal Analysis (DTA), and Differential Scanning Calorimetry (DSC) were carried out with a SDT Q600 V20.9 build 20 instrument using a 10 K/min heating rate. The thermal treatment applied to as-spun samples for obtaining dense ceramic fibers consisted in four different stages at 800, 1000, 1200 and 1400 °C. The treated samples were characterized by FTIR, SEM, Raman spectroscopy using a 532 nm laser scanning an area of 5 μm, and crystalline phases were identified by XRD with a X'Pert PRO PANalytical diffractometer ($CuK\alpha_1$, 35 kV, 25 mA) with scanning range from 20 to 80° and 2°/min scan speed.

III. Results and Discussion

(1) Preparation of precursor solutions

Different issues were observed during the preparation of precursor solutions. Strontium nitrate is partially soluble in acetic acid and ethanol, so it was necessary to add water to obtain the precursor solutions. This step differs from Macaraig *et al.* [1]. However, the amount of water that can be used is limited, because titanium tetraisopropoxide might form gels. This issue was overcome by dissolving strontium nitrate in water before addition of acetic acid. After this, the time required for preparation and homogenization decreased. The use of strong acid improved hydrolysis of alcoxides, as reported by Llano *et al.* [9]. The dissolution of titanium tetraisopropoxide was faster than using acetic acid. However, concentrated hydrochloric acid reacted with PVP and caused its peptization, as described by Yoshida and Prasad [10]. Diluted acid was used to avoid polymer peptization, but the resulting sol-gel was not suitable for electrospinning. A 0.25 M was prepared, according to works reported by Macaraig *et al.* [1], to improve the structure of green fibers, yet not important changes were observed. As a result, a solution of higher concentration was chosen. 0.3 M was selected as the maximum concentration because solubility of strontium titanate in water is low and precipitates may form, as reported by Wang *et al.* [11]. Concerning this issue, it has been previously reported that precursor concentration is a crucial parameter for the efficient preparation of fibers by electrospinning and sol-gel because it affects viscosity and surface tension. In the specific case of ceramics, it has been observed that characteristics like diameter, grain growth rate, and sinterability are influenced by concentration values. The effects of concentration on fibrous morphology are caused by the accumulation of higher electric charge once voltage was applied due to the abundance of solutes [12–15].

Fig. 1 shows SEM images of as-spun fibers prepared using precursor solution M1. In the image at 5,000X (fig. 1a), beads with irregular shape were observed. These defects are generated by the increase in viscosity due to polymerization of ceramic precursor during sol-gel process. At 20,000X (fig. 1b), it was observed that the obtained samples consisted in continuous, uniform, non-aligned fibers, with smooth surface and mean diameter of 140±35 nm. EDX of samples obtained from M1 is presented in Fig. 1c. Titanium and Strontium were present in very low proportions because in this stage the precursor fibers are composed mainly by polymer. EDX showed that Carbon and Oxygen represented 61.73 and 24.60 wt%, respectively, followed by Nitrogen (12.30 wt%). By contrast, Titanium (1.32 wt%) and Strontium (0.05%) are present in the lowest proportions. Signals at 1.8 and 14.14 keV correspond to Sr atoms, while 0.45 and 4.50 keV signals belong to Titanium. Oxygen, Carbon, and Nitrogen are identified by the signals at 0.52, 0.27 and 0.29 keV, respectively.

Fig. 2 shows samples obtained from solution M2 aged for 24 h. Clear beads of irregular shape are present in the image at 5,000X (fig. 2a). The spherical defects observed in SEM images were caused by instability of Taylor cone during electrospinning [8]. Another factor influencing the formation of defects is relative humidity. High percentages of environmental humidity inhibit evaporation of solvents during the migration of precursor solution from needle tip to collector [12]. Furthermore, this parameter affects viscosity by increasing attraction between molecules. The third factor that influenced structure and morphology of fibers and defects is voltage. It was observed that at high voltages the imperfections tend to elongate, while at low values defects are spherical [13]. Fig. 2-b (20,000X) shows aligned continuous fibers with mean diameter of 180±59 nm. EDX of as-spun fibers obtained from solution M2 is shown in Fig. 2-c. In this sample, presence of peaks corresponding to titanium and strontium is small, because the fibers were composed mainly of polymer (PVP). According to this analysis, Carbon and Oxygen represent 77.23 wt%

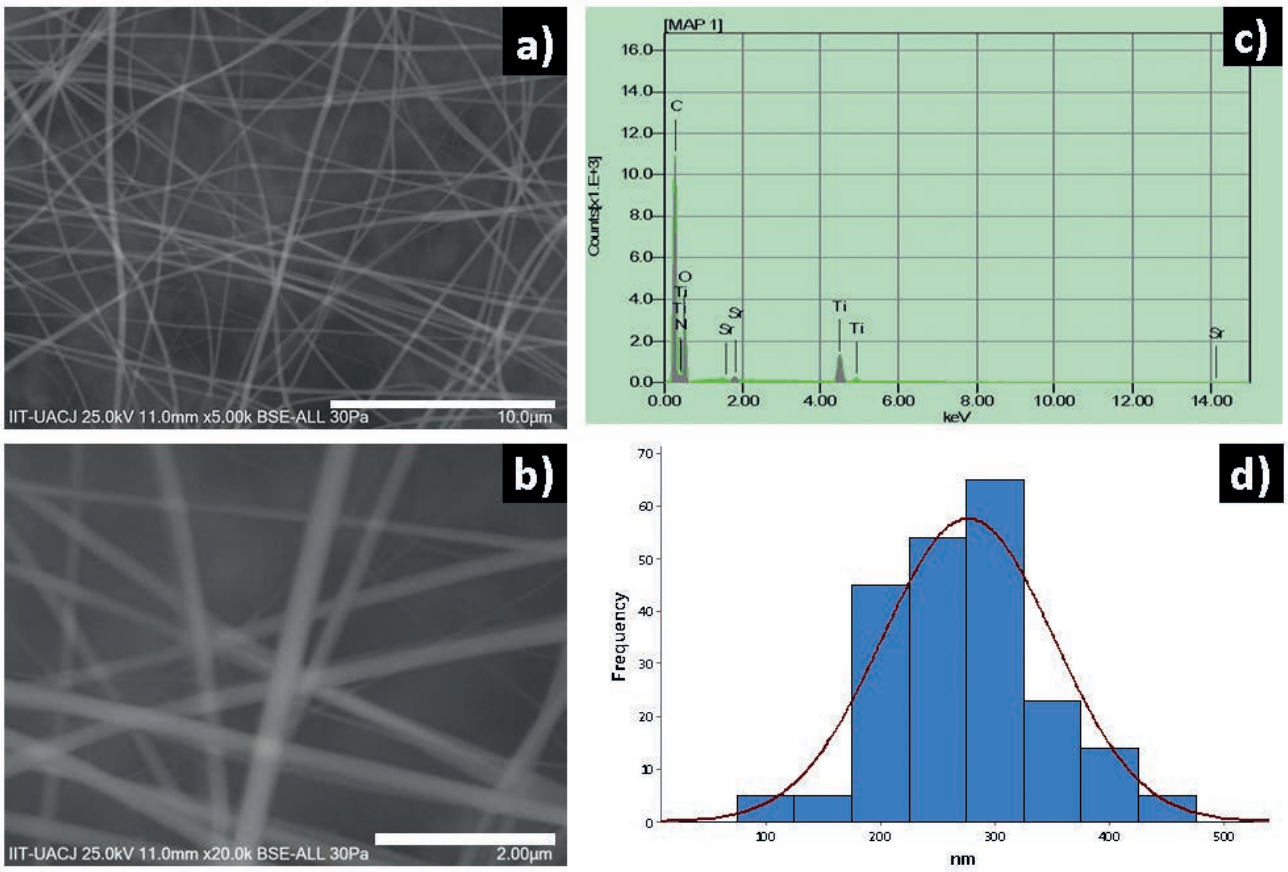

Fig. 1: SEM images of as-spun green fibers obtained from M1: a) 5,000X, b) 20,000X, c) EDX spectrum and d) Histogram.

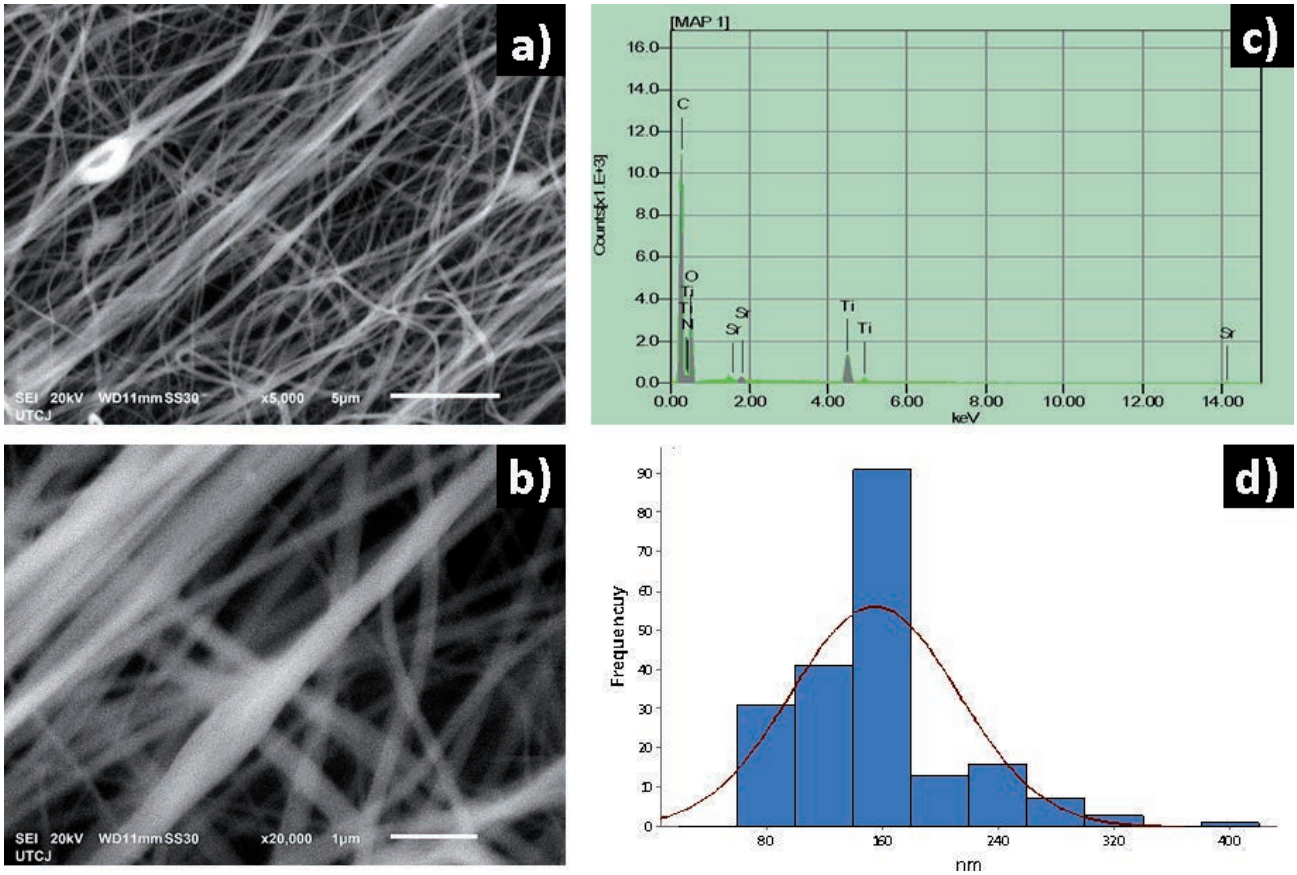

Fig. 2: SEM images of as-spun green fibers obtained from M2 aged 24 h: a) 5,000X, b) 20,000X, c) EDX spectrum and d) Histogram.

and 22.11 wt%, respectively. By contrast, Titanium corresponded to only 0.66 wt% and strontium 0.03 wt%. Signals detected at 0.45 keV and 4.50 keV correspond to Titanium, whereas those at 0.52 keV and 0.27 keV represent Oxygen and Carbon, respectively.

IV. Infrared Spectroscopy

Fig. 3 shows infrared spectra of as-spun green fibers M1 and M2. As observed, there are no differences between the spectra of the two samples. At 25 °C the spectra show absorption bands related to functional groups in the PVP, a hydroxyl stretching band of H_2O is present at 3420 cm^{-1}, followed by C-H stretching bands at 2900 cm^{-1}. Most characteristic PVP bands are observed in the fingerprint zone in the range from 1200 to 1700 cm^{-1}. In this zone, the stretching of carbonyl (C=O) bonds can be observed at 1655 cm^{-1}, while scissoring bands of methyl groups are present at 1441, 1415 and 1379 cm^{-1}, the characteristic vibration of the C=O group appears at 1291 cm^{-1}, and 650 cm^{-1} corresponds to the nitrogen of the tertiary amine in PVP, while scissoring bending vibration of N-H bonds is observed at 1550 cm^{-1}. Asymmetric stretching of C-N and C-C bonds is represented by bands placed at 1450 and 1238 cm^{-1}, respectively. The band at 823 cm^{-1} represents symmetric stretching of C-H bonds. All these bonds and functional groups belong to the polymer used in the fabrication of as-spun fibers. Inorganic species are observed in the zone between 500 – 800 cm^{-1}. Sr-O asymmetric stretching is located at 745 cm^{-1}. Asymmetric stretching of Ti-O-Ti and Ti-O bonds is represented by vibration bands at 680 and 560 cm^{-1}, respectively [16–17]. Vibration bands corresponding to PVP and inorganic species are shown in Table 1. As observed in the image, bands generated by hydroxyl groups (OH) are present in both samples. These signals are caused by the water used in the preparation of the precursor sol-gel. PVP bands show the same intensities because the concentration used was constant.

Table 1: Characteristic infrared vibration bands of PVP and inorganic species.

Wavenumber (cm^{-1})	Bonds
1640	C=O V_s
1550	NH_2 δ
1450	C— N— C V_{as}
1238	C— C V_{as}
823	C— H V_s
745	Sr— O V_{as}
680	Ti— O — Ti V_{as}
560	Ti— O V_{as}

δ scissoring bending; V_{as} asymmetric stretching; V_s symmetric stretching

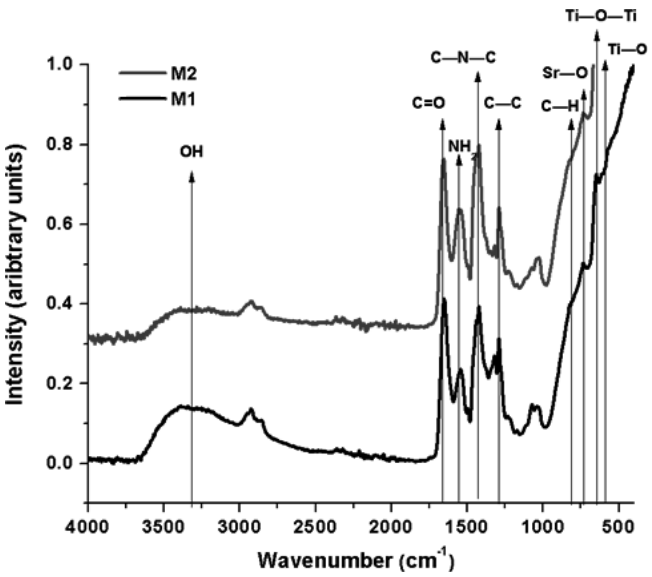

Fig. 3: Infrared spectra of as-spun green fibers obtained using solutions M1 and M2. Characteristic bands of strontium titanate can be observed.

V. Thermal Analyses

Thermogravimetric analysis (TGA) of fibers obtained from solution M1 is shown in Fig. 4. The first weight loss of 18% occurs from 20 – 200 °C and is caused by the elimination of structural water. Thermal decomposition of organic matter and generation of CO_2 took place between 350 and 480 °C with weight loss of 43%, with an inflection point at 425 °C. The maximum weight loss is observed at 640 °C, which represents the elimination of N_2 and the complete thermal decomposition of organic material, corresponding to a weight loss of 50%. The analysis reveals that after heat treatment under a temperature of 900 °C, the composite loses up to 50% of its weight. Weight does not vary greatly from 640 to 1100 °C. However, after this point sample gains 30% of weight until 1400 °C. The final mass, representing 73% of the original value, is caused

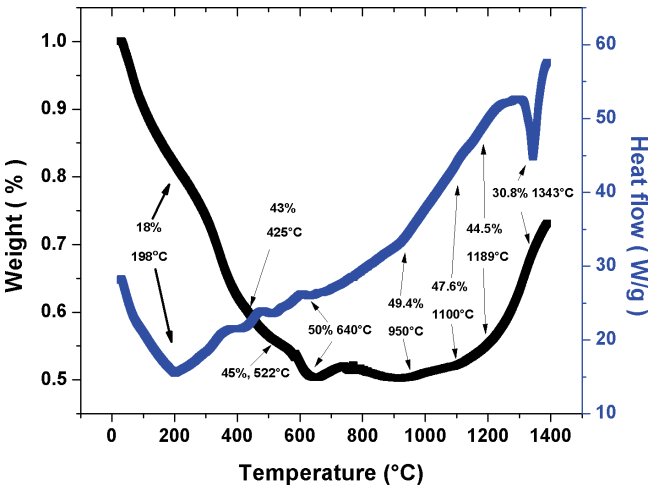

Fig. 4: TGA (black) and DSC (blue) thermogram of as-spun fibers obtained from M1.

by oxidation of the ceramic material. In Fig. 4, the results obtained by DSC are shown. Structural water was lost between 200 and 300 °C, while decomposition of organic material was observed at 400 – 480 °C with an inflection point at 425 °C. Elimination of N_2 is represented by the zone at 560 – 640 °C, with a minimum at 600 °C [16–18]. Sintering of the ceramic material is observed as an endothermic peak around 1343 °C.

VI. Thermal Treatment

Fig. 5 shows infrared spectra, in the interval from 800 – 400 cm^{-1}, of samples treated at four different temperatures. The sample obtained from solution M2 was characterized because this precursor solution allowed a better electrospinning and gives uniform fibers after thermal treatment since the aging of the solution increases the resistance of the fibers. The bands at 745, 680, and 540 cm^{-1} correspond to Sr-O $_{Vas}$, Ti-O-Ti $_{Vas}$, and Ti-O $_{Vas}$ bonds, respectively. Those bands are characteristic of Strontium titanate [17–19]. Sr-O and Ti-O-Ti bands are overlapped, while a weak band at 560 cm^{-1} is observed at 800 °C. At 1000 and 1200 °C, intensity of the band representing Ti-O increased. By contrast, Ti-O bands are lost at 1400 °C.

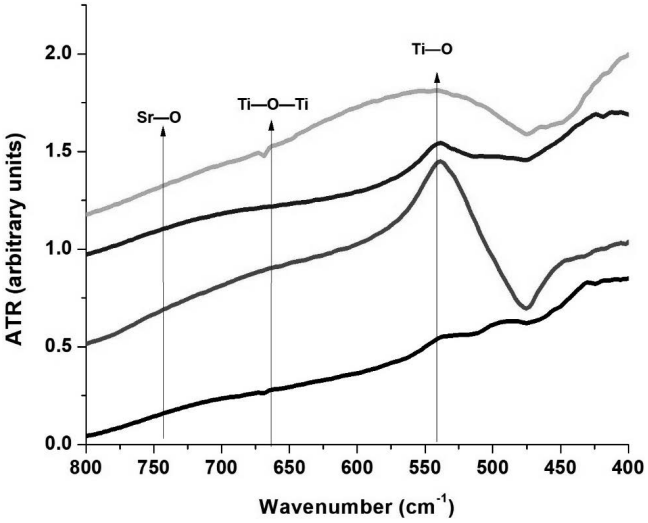

Fig. 5: Amplification of infrared spectra of M2 sample treated at different temperatures, in the range from 800 – 400 cm^{-1}: 800 °C (black), 1000 °C (red), 1200 °C (blue), and 1400 °C (green).

VII. Raman Spectroscopy

Fig. 6 shows Raman spectra of samples obtained from solution M2, after thermal treatment at 800, 1000, and 1200 °C. Bands between 85 and 139 cm^{-1} correspond to TO_1, while TO_2 and LO_1 are represented at 240 cm^{-1} [20]. Furthermore, LO_3 and TO_4 are represented by bands at 440 cm^{-1} and 610 cm^{-1}, respectively. The later values are different from previous works [20], in which LO_3 and TO_4 were observed at 480 cm^{-1} and 550 cm^{-1}. The shift in Raman bands can be attributed to TiO_2 impurities in samples. This ceramic presents Raman bands located at 447 cm^{-1} and 612 cm^{-1}, according to Ohsaka *et al.* [21]. Bands shape and intensity are influenced by type of laser used. A Stokes shift can be generated by a 325 nm laser, causing the shift and increment of Raman bands [22]. The observed bands are characteristic of strontium titanate with Perovskite structure [20]. Bands located between 80 – 125 cm^{-1} are overlapped because definition increases due to exposition time. All these bands are present in the spectra, which demonstrates that chemical bonds were not affected by the treatment at three different temperatures.

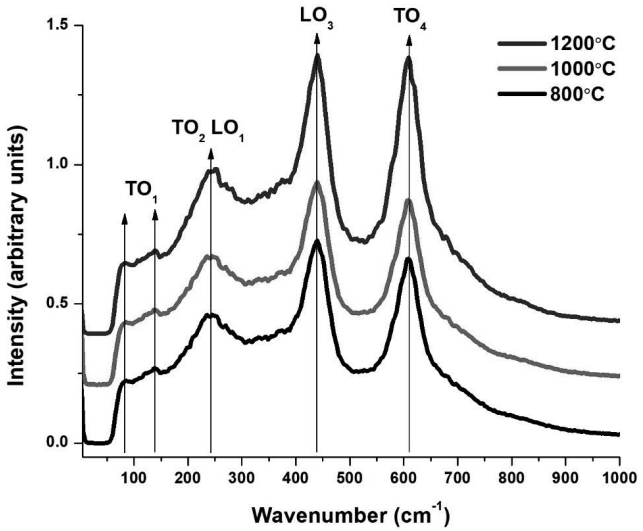

Fig. 6: Raman spectra of M2 sample treated thermally at 800, 1000 and 1200 °C.

VIII. X-Ray Diffraction

X ray diffraction patterns of samples obtained from solution M2 after the thermal treatment at 800, 1000 and 1200 °C are shown in Fig. 7. At a higher temperature of 600 °C, maximum of the organic material was removed from the fibers according TGA and DSC analysis. Strontium titanate characteristic peaks are observed at 23, 32, 40, 47, 58, 69 and 77°, which represent the planes (100), (110), (111), (200), (210), (220), and (310), respectively. [23–24]. At 800 °C, the characteristic planes of perovskite structure are observed [25]. However, planes corresponding to two different TiO_2 phases are observed, as reported

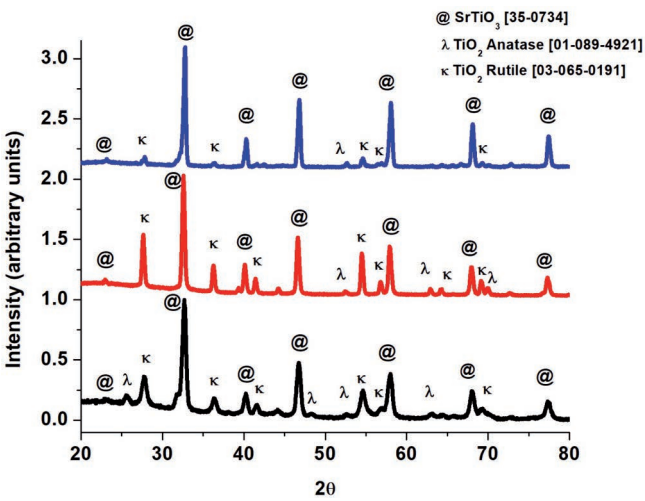

Fig. 7: XRD pattern of Strontium titanate fibers at 800 °C (black), 1000 °C (red) and 1200 °C (blue).

by Malgahães *et al.* [26]. At 800 °C, small anatase planes (101), (200), (105), (204), (220) are observed at 26, 48, 53, 64, and 71°, respectively [JCP:01 – 089 – 4921]. By contrast, rutile phase [JCP:03 – 065 – 0191] is identified by crystallographic peaks at 27.7, 36.2, 41.7, 54.7, 56.9 and 69.2°, representing the planes (110), (101), (111), (211), (220), and (301), according to previous reports [27 – 28]. At 1000 °C the perovskite structure characteristic of strontium titanate was present in a high proportion.

However, the peaks of tetragonal TiO_2 (anatase) lost intensity as temperature increased indicating the transition to rutile and a greater incorporation of Ti to $SrTiO_3$. Only a small peak of anatase is observed at 1200 °C. In comparison, intensity and definition of rutile peaks increased in samples treated at 1000 °C because this crystalline phase is more stable at high temperatures. However, at 1200 °C only small peaks of both TiO_2 polymorph are observed together with well-defined and intense strontium titanate peaks [27 – 28].

Fig. 8 shows SEM images of sample obtained from solution M2 after treating at 800 °C. At 10,000X, it was observed that fibers were not aligned, and some white beads were present (fig. 8a). The image at 50,000X (fig. 8b) shows continuous fibers with smooth surface. Mean diameter decreased to 95±25 nm due to the thermal decomposition of PVP and keeps constant along the fiber. EDX of fibers obtained from M2 treated at 800 °C is shown in Fig. 8c.

In contrast with non-treated samples, weight percentage attributed by metal elements was higher. Strontium and Titanium represented 1.90 wt% and 5.34 wt%, respectively, while Oxygen corresponded to 22.24 wt%. Nitrogen was not detected because of polymer decomposition. The high Carbon percentage detected (70.53 wt%) was caused by the tape used for mounting the sample. Signals at 1.8 and 14.14 keV correspond to strontium, while titanium is detected at 0.45 and 4.50 keV. Oxygen and carbon are placed at 0.52 and 0.27 keV, respectively.

Fig. 9 shows fibers obtained from solution M2 and treated at 1000 °C. Mean diameter increased to 103±39 nm, compared to previous stage. Sintering centers with smooth surface and round shape are observed at 5,000X (fig. 9a). These defects grew from the beads present at 800 °C. In the image at 10,000X, it was observed that some fibers were broken (fig. 9b). The strontium titanate fibers maintain its characteristic morphology at 1000 °C. By contrast, morphology was affected when samples were treated at higher temperatures. Therefore, 1000 °C was selected as the optimal temperature for the fabrication of dense strontium titanate fibers.

Fig. 10 shows samples obtained from solution M2 and treated at 1200 °C. Sintering process started at this temperature and fibrous morphology was affected, as observed at 5,000X (fig. 10a). In some areas, particles and agglomerations are present. However, grain growth was slower compared to previous temperature. At 10,000X (fig. 10c), continuous fibers with smooth surface and mean diameter of 137±43 nm were observed.

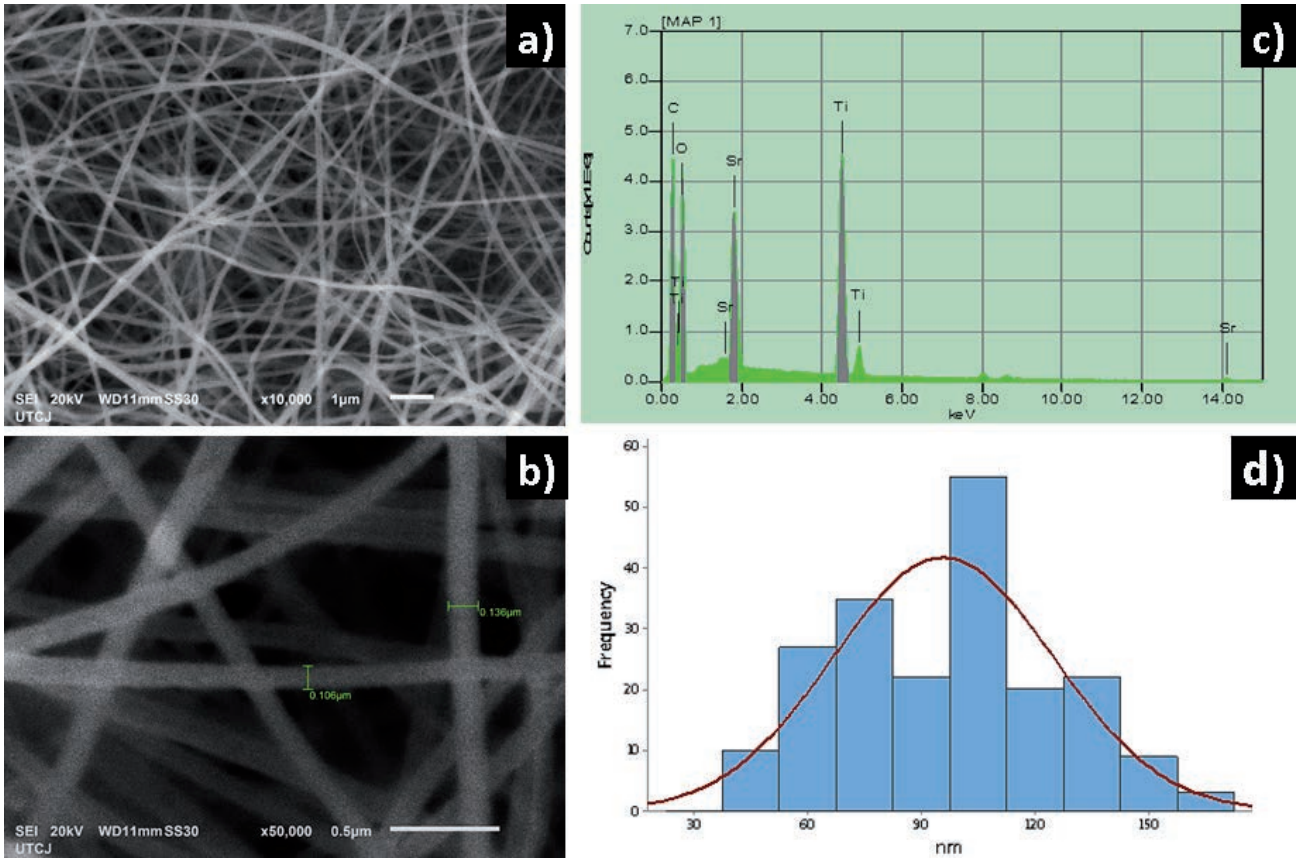

Fig. 8: SEM images of Strontium titanate fibers after thermal treatment at 800 °C: a) 10,000X; b) 50,000X, c) EDX spectrum and d) Histogram.

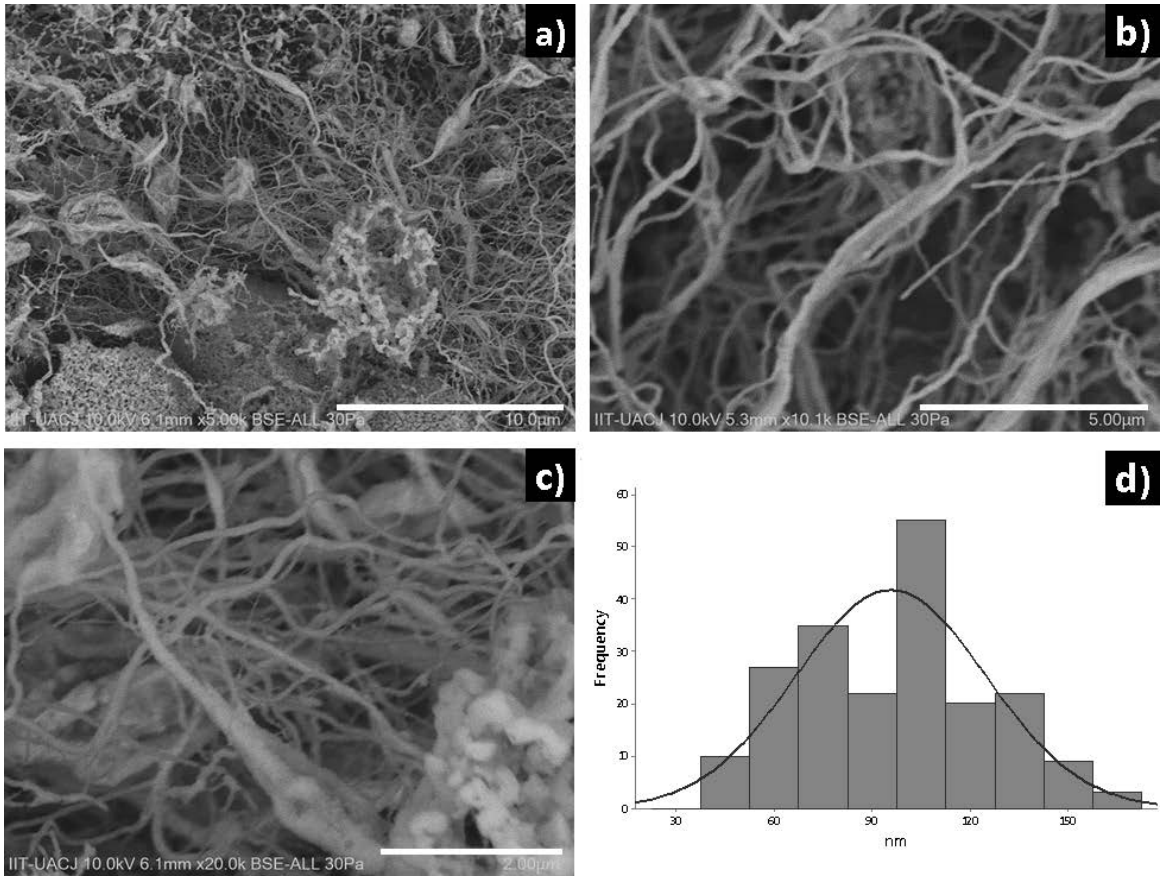

Fig. 9: SEM images of Strontium titanate fibers after thermal treatment at 1000 °C: a) 5,000X, b) 10,000X, c) 20,000X and d) Histogram.

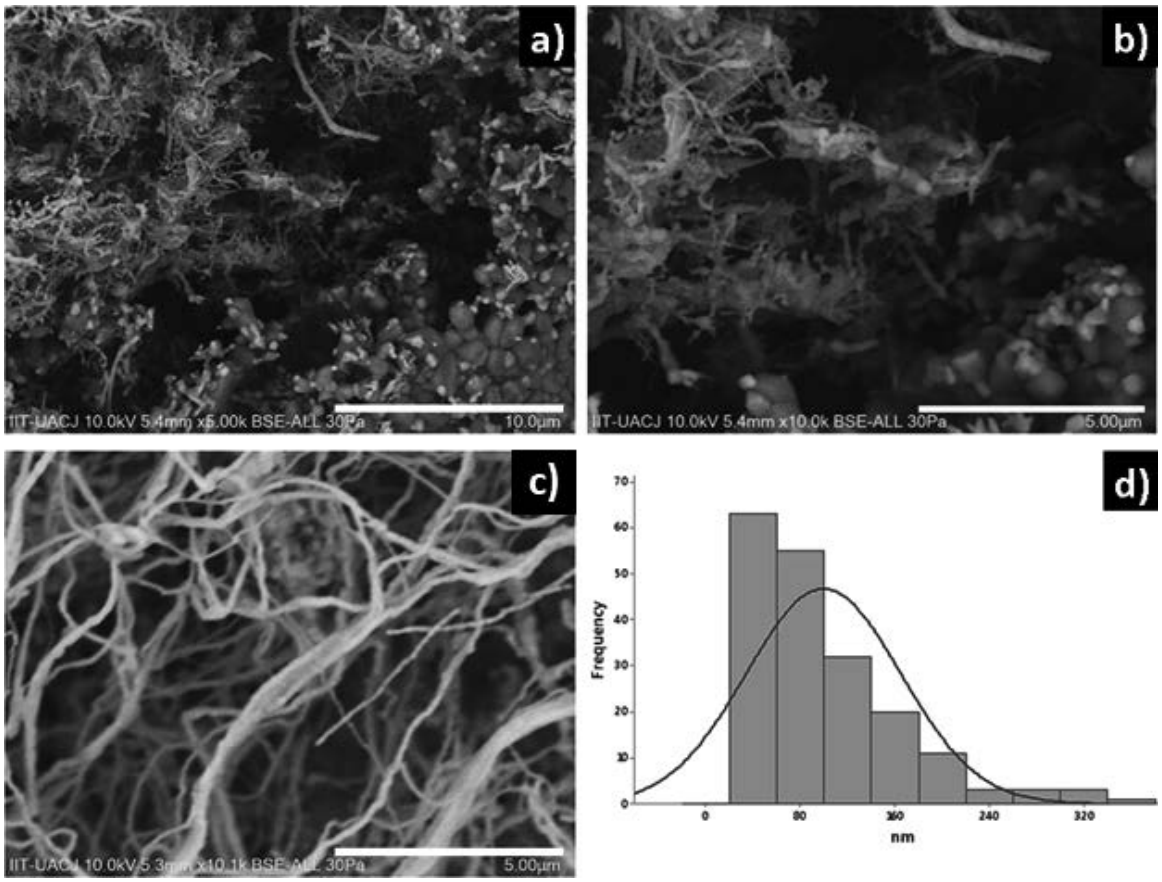

Fig. 10: SEM images of strontium titanate fibers after thermal treatment at 1200 °C: a) 5,000X, b) 10,000X, c) 10,000X and d) Histogram.

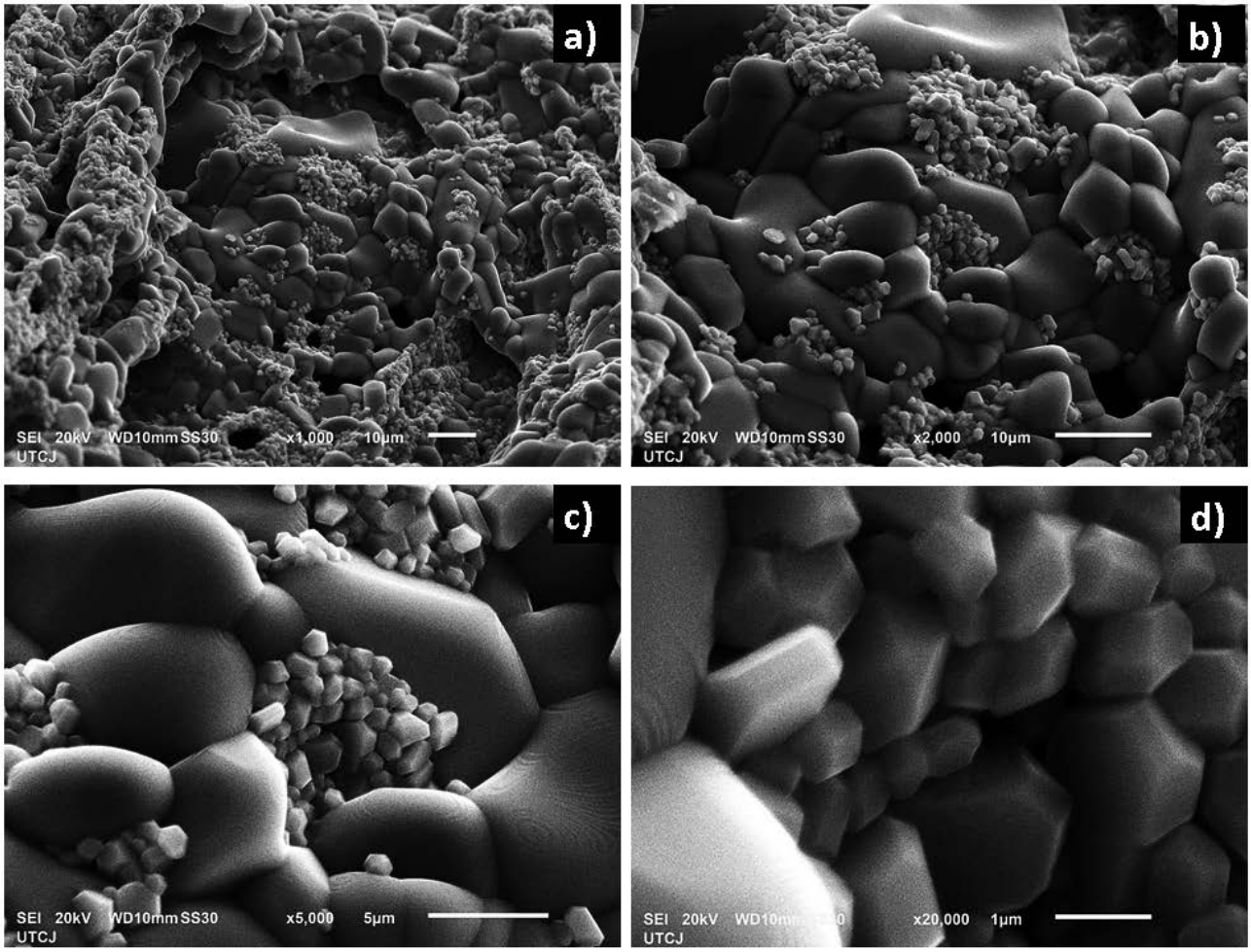

Fig. 11: SEM images of Strontium titanate samples after thermal treatment at 1400 °C: a) 1,000X, b) 2,000X, c) 5,000X and d) 20,000X.

Fig. 11 shows samples after thermal treatment at 1400 °C. As observed in the image, fibrous morphology was lost. Instead, ceramic particles with mean diameter of 607±384 nm were obtained due to sintering process and grain growth [14]. A strontium titanate film began to form due to grain growth and sintering processes. Hexagonal structures were observed, which are characteristic of strontium titanate particles, as reported by Dong *et al.* [29].

In addition, it was observed that strontium titanate samples treated at 1400 °C presented higher mechanical strength that the samples treated at lower temperatures. As demonstrated by XRD, the proportion of titania crystalline phases decreases with temperature, while strontium titanate increased. Therefore, at 1400 °C sample was composed completely of this ceramic. The biggest particles present in the image were formed by sintering of smaller grains.

IX. Conclusions

An alternative methodology was obtained for the synthesis of strontium titanate fibers, which combines the sol-gel and electrospinning technique to produce a fibrillar ceramic composite. A mean diameter of 103±39 nm was obtained using a 0.30 M precursor solution. Precursor concentration influenced morphology and stability of samples, as homogenous and smooth fibers were obtained from more concentrated solutions. The characteristic bands of strontium titanate of perovskite structure were identified in Infrared and Raman spectroscopy. The presence of tetragonal titania and strontium titanate was demonstrated at 800 °C by thermal analyses and X-ray diffraction. At 1200 °C, tetragonal TiO_2 decreased and pure and crystalline strontium titanate was observed.

Acknowledgments

Thanks to PRODEP, Universidad Autónoma de Ciudad Juárez and CONACYT for supporting these investigations.

References

1 Macaraig, L., Chuangchote, S., Sagawa, T.; Electrospun $SrTiO_3$ nanofibers for photocatalytic hydrogen generation. J. of Mater. Res., **29**, 123 – 130 (2014).

2 Klein, C., Hurlbut, C. S., Manual de mineralogía Vol. 2, Reverte, España (1996).

3 Roque-Ruiz, J. H., Cabrera-Ontiveros, E. A., Torres-Pérez, J., Reyes-López, S. Y (2016). Preparation of PCL/clay and PVA/clay electrospun fibers for Cadmium (Cd^{+2}), Chromium (Cr^{+3}), Copper (Cu^{+2}) and Lead (Pb^{+2}) removal from water. Water, Air, Soil Poll., **227**, 286 (2016).

4 Li, D., Xia, Y., Electrospinning of nanofibers: Reinventing the wheel. Adv. Mater., **16**, 1151 – 1170 (2004).

5 Bhardwaj, N., Kundu, S. C. Electrospinning: A fascinating fiber fabrication technique. Biotechn. Adv., **28**, 325 – 347 (2010).

6 Reyes-López, S. Y., Cornejo-Monroy, D., González-García, G. A novel route for the preparation of gold nanoparticles in polycaprolactone nanofibers. J. of Nanomater., **16**, 153 (2015).

7 López-Esparza, J., Espinosa-Cristóbal, L. F., Donohue-Cornejo, A., Reyes-López, S. Y., Antimicrobial activity of silver nanoparticles in polycaprolactone nanofibers against gram-positive and gram-negative bacteria. Ind. Eng. Chem. Res., **55**, 12532 – 12538 (2016).

8 Garibay-Alvarado, J. A., Espinosa-Cristóbal, L. F., &. Reyes-López Y. S. Fibrous silica-hydroxyapatite composite by electrospinning. Int. J. Res. GRANTHAALAYAH. **5** (2017).

9 Llano, B., Marín, J. M., Restrepo, G., Ríos, L. A. Síntesis, caracterización y evaluación fotocatalítica de óxidos mixtos titanio-silicio. Sci. Techn., **1** (2007).

10 Yoshida, M., Prasad, P. N. Sol-gel-processed SiO_2/TiO_2/poly (vinylpyrrolidone) composite materials for optical waveguides. Chem. Mater., **8**, 235 – 241 (1996).

11 Wang, X., Zhang, L., Liu, H., Zhai, J., Yao, X. Dielectric nonlinear properties of $BaTiO_3$-$CaTiO_3$-$SrTiO_3$ ceramics near the solubility limit. Mater. Chem. Phys., **112**, 675 – 678 (2008).

12 Nezarati, R. M., Eifert, M. B., Cosgriff-Hernandez, E., Effects of humidity and solution viscosity on electrospun fiber morphology. Tissue Eng. C, Methods, **19**, 810 – 819 (2013).

13 Huan, S., Liu, G., Han, G., Cheng, W., Fu, Z., Wu, Q., Wang, Q., Effect of experimental parameters on morphological, mechanical and hydrophobic properties of electrospun polystyrene fibers. Mater., **8**, 2718 – 2734 (2015).

14 Roque-Ruiz, J. H.; Medellín-Castillo, N. A.; Reyes-López, S. Y., Fabrication of α-alumina fibers by sol-gel and electrospinning of aluminum nitrate precursor solutions. Res. Phys. **12**, 193 – 204 (2019).

15 Garibay-Alvarado, J. A., Farias, R., Reyes-López, S. Y., Sol-gel and electrospinning synthesis of lithium niobate-silica nanofibers. In press, Coatings, **9** (2019).

16 Uddin, M. E., Layek, R. K., Kim, N. H., Hui, D., Lee, J. H., Preparation and properties of reduced graphene oxide/polyacrylonitrile nanocomposites using polyvinyl phenol. Compos. B, Eng., **80**, 238 – 245.M (2015).

17 Kong, J., Rui, Z., Ji, H., Carbon nitride polymer sensitization and nitrogen doping of $SrTiO_3/TiO_2$ nanotube heterostructure toward high visible light photocatalytic performance. Ind. Eng. Chem. Res., **56**, 9999 – 10008 (2017).

18 Tang, Y., Xie, L., Sai, M., Xu, N., Ding, D., Preparation and antibacterial activity of quaternized chitosan with iodine. Mater. Sci. Eng. C, **48**, 1 – 4 (2015).

19 George, C. N., Thomas, J. K., Jose, R., Kumar, H. P., Suresh, M. K., Kumar, V. R., Koshy, J., Synthesis and characterization of nanocrystalline strontium titanate through a modified combustion method and its sintering and dielectric properties. J. Alloys and Comp., **486** (1 – 2), 711 – 715 (2009).

20 Tenne, D. A., Farrar, A. K., Brooks, C. M., Heeg, T., Schubert, J., Jang, H. W., Schlom, D. G., Ferroelectricity in nonstoichiometric $SrTiO_3$ films studied by ultraviolet Raman spectroscopy. Appl. Phys. Lett., **97**, 142901 (2010).

21 Ohsaka, T., Izumi, F., Fujiki, Y., Raman spectrum of anatase, TiO_2. J. Raman spectroscopy, **7**, 321 – 324 (1978).

22 Basiev, T. T., Sobol, A. A., Zverev, P. G., Osiko, V. V., Powell, R. C., Comparative spontaneous Raman spectroscopy of crystals for Raman lasers. Appl. Opt., **38**, 594 – 598 (1999).

23 Hao, J. H., Gao, J., Wong, H. K., Laser molecular beam epitaxy growth and properties of $SrTiO_3$ thin films for microelectronic applications. Thin Solid Films, **515**, 559 – 562 (2006).

24 Singh, D. K., Manam, J., Optical spectroscopic and thermal quenching behaviour of perovskite $SrTiO_3$: Sm^{3+} orange emitting phosphors for lighting applications. J. Mater. Sci.: Materials in Electronics, **29**, 5579 – 5588 (2018).

25 Su, E. C., Huang, B. S., Wey, M. Y., Enhanced optical and electronic properties of a solar light-responsive photocatalyst for efficient hydrogen evolution by $SrTiO_3/TiO_2$ nanotube combination. Solar Ener., **134**, 52 – 63 (2016).

26 Magalhães, R. S., Junior, W. D., Souza, A. E., Teixeira, S. R., Li, M. S., Longo, E., Synthesis of $BaTIO_3$ and $SrTIO_3$ by microwave assisted hidrotermal method (mah) using anatase as titanium precursor. Química Nova, **40**, 166 – 170 (2017).

27 Zavala, M. Á. L., Morales, S. A. L., Ávila-Santos, M., Synthesis of stable TiO_2 nanotubes: Effect of hydrothermal treatment, acid washing and annealing temperature. Heliyon, **3**, e00456 (2017).

28 Roque-Ruiz, J. H., Martínez-Máynez, H., Zalapa-Garibay, M. A., Arizmendi-Moraquecho, A., Farias, R., Reyes-López, S. Y., Surface enhanced Raman spectroscopy in nanofibers mats of SiO_2-TiO_2-Ag. Res. Phys., **7**, 2520 – 2527 (2017).

29 Dong, L., Luo, Q., Cheng, K., Shi, H., Wang, Q., Weng, W., Han, W. Q. Facet-specific assembly of proteins on $SrTiO_3$ polyhedral nanocrystals. Sci. Rep., **4**, 5084 (2014).